photochem

MDPI

Article

Mass-Resolved Momentum Imaging of Three Dichloroethylene Isomers by Femtosecond Laser-Induced Coulomb Explosion

Yoriko Wada [1], Hiroshi Akagi [1], Takayuki Kumada [2], Ryuji Itakura [1] and Tomonari Wakabayashi [3,*]

[1] Kansai Photon Science Institute, National Institutes for Quantum Science and Technology, Kizugawa 619-0215, Japan
[2] Japan Atomic Energy Agency, Tokai-mura, Ibaraki 319-1195, Japan
[3] Department of Chemistry, School of Science and Engineering, Kindai University, Higashi-Osaka 577-8502, Japan
* Correspondence: wakaba@chem.kindai.ac.jp; Tel.: +81-6-4307-3408

Abstract: Coulomb explosion experiments using linearly polarized intense 60 fs laser pulses were conducted for structural characterization of three dichloroethylene (DCE) isomers, 1,1-DCE, *cis*-1,2-DCE, and *trans*-1,2-DCE. Under relatively low laser intensity at 1.8×10^{14} W/cm^2, mass-resolved momentum imaging (MRMI) for selected fragment ions of $^{35}Cl^+$ and C^{2+} revealed different patterns for the three isomers. The C^{2+} ion fragmented from multiply charged *trans*-1,2-DCE was forced to leave perpendicularly to the direction of the laser polarization, due to recoil forces from adjacent cations. In contrast, the fast ions of C^{2+} from *cis*-1,2-DCE exhibited an isotropic distribution, whereas the fast ions of C^{2+} from 1,1-DCE recoiled along the laser polarization together with the slow C^{2+} ions, and thereby distinction of the three isomers was demonstrated. Coulomb explosion occurs predominantly at specific orientation, which is useful for potential applications of MRMI analysis to molecular structure assays.

Keywords: dichloroethylene isomers; femtosecond laser; coulomb explosion; mass-resolved momentum imaging; molecular structure assay

check for updates

Citation: Wada, Y.; Akagi, H.; Kumada, T.; Itakura, R.; Wakabayashi, T. Mass-Resolved Momentum Imaging of Three Dichloroethylene Isomers by Femtosecond Laser-Induced Coulomb Explosion. *Photochem* **2022**, *2*, 798–809. https://doi.org/10.3390/photochem2030051

Academic Editors: Rui Fausto and Robert Kołos

Received: 18 August 2022
Accepted: 13 September 2022
Published: 16 September 2022

Publisher's Note: MDPI stays neutral with regard to jurisdictional claims in published maps and institutional affiliations.

Copyright: © 2022 by the authors. Licensee MDPI, Basel, Switzerland. This article is an open access article distributed under the terms and conditions of the Creative Commons Attribution (CC BY) license (https://creativecommons.org/licenses/by/4.0/).

1. Introduction

Coulomb explosion is a molecular process in a multiply charged ion, resulting in explosive release of fragment ions by their Coulomb repulsion. Tracing back trajectories of the fragment ions, molecular structure of the nascent parent ion can be reconstructed to understand the structure and dynamics of the multiply charged ion. Coulomb explosion imaging (CEI) is a technique pioneered by Naaman and co-workers to study geometric structures of small molecules, where valence electrons are stripped off from a projectile ion by a thin foil of gold [1]. This technique has been developed to identify each of the chiral pair of epoxide molecules [2]. Momentum analysis of fragment ions by CEI has been applied by introducing intense ultrafast laser pulses for ionization [3–10]. Thus far, applications are found for small molecules such as water vapor molecules, H_2O [3] and D_2O [4], sulfur dioxide, SO_2 [4], carbon disulfide, CS_2 [5], dichloromethane, CH_2Cl_2 [6], and weakly bound clusters of N_2Ar, O_2Ar, and O_2Xe [7]. This has been extended to relatively large molecules of 3,5-dibromo-3′,5′-difluoro-4′-cyanobiphenyl [8] and group-6 metal hexacarbonyls, $Cr(CO)_6$, $Mo(CO)_6$, and $W(CO)_6$ [9].

Structural characterization of reactive chemical species such as atomic clusters and reaction intermediates has long been a central subject in chemistry, where fragility and reactivity have thwarted attempts to make a crystalline form necessary for the X-ray diffraction analysis to identify definite molecular structures [11,12]. As a recent example, we refer to a series of photo-sensitive sp-conjugated polyyne-iodine adducts, $C_{2n}H_2I_6$ (n = 5–9), which have been identified only in solutions by UV–VIS absorption, ^{13}C-NMR, and infrared absorption (FTIR) spectroscopy [13–15]. Despite the analysis of chemical shifts [13] and vibrational-mode frequencies [14], positions of six iodine atoms in the molecular adduct,

namely, the molecular structure, could not be located unequivocally on the experimental bases. Recently, an sp-hybridized carbon molecule of diiodediacetylene, $I(C{\equiv}C)_2I$, has been studied by Coulomb explosion experiments to find anisotropic angular distribution of fragment ions [16]. The experimental results imply that Coulomb explosion experiments would be able to characterize the structure of such fragile or reactive molecules, if they could be introduced into a high vacuum. For the investigation of molecular structures in such complexes as organic halogen adducts, we focus herein on the gas phase experiment utilizing mass-resolved momentum imaging (MRMI) for fragment ions generated upon Coulomb explosion.

Characterization of isomeric forms in a molecular species is one of the challenging issues in Coulomb explosion experiments [17–25]. Thus far, distinction of enantiomers of CHBrClF and $CF_3CHBrCl$ has been reported [17–19]. Instantaneous chirality induced by zero-point vibrations has been observed for a symmetric molecule of CD_4 [20]. For structural isomers, distinction of 2,6- and 3,5-difluoroiodobenzene isomers has been demonstrated [21]. Recently, laser-induced alignment has been combined with CEI for determination of enantiomeric state of an axially chiral molecule (3,5-dibromo-3′,5′-diflouro-4′-cyanobiphenyl molecule) [22], and identification of difluoroiodobenzene isomers [23] and dihydroxybromobenzene isomers [23]. Yatsuhashi et al. conducted Coulomb explosion experiments on the isomers of dichloroethylene (DCE) $C_2H_2Cl_2$, namely, 1,1-DCE, *cis*-1,2-DCE, and *trans*-1,2-DCE, using linearly polarized intense femtosecond laser pulses [24]. From dissimilarity observed for angular distributions of fragment ions, e.g., $^{35}Cl^{y+}$ (y = 1,2), $^{12}C^{z+}$ (z = 2,3), and H^+, the authors concluded that *trans*-1,2-DCE was clearly distinguishable from the other two [24]. Additionally, for a similar species of dibromoethylene $C_2H_2Br_2$, the *cis*-1,2 and *trans*-1,2 isomers have been identified with X-ray-induced Coulomb explosion, but the 1,1-isomer has not been treated [25]. In order to complete a protocol for discrimination of all the three isomers in DCE, an additional tool is necessary for distinction between the two isomers, *cis*-1,2-DCE and 1,1-DCE.

In this work, three isomers of DCE were examined by the momentum imaging for fragment ions, on the basis of new experimental data from laser-induced Coulomb explosion. In addition to a similar laser-intensity condition to the previous experiments [24], 1.7×10^{15} W/cm^2 (1.7 PW/cm^2), we studied a condition of an order-of-magnitude-lower intensity, 1.8×10^{14} W/cm^2 (0.18 PW/cm^2), where saturation of ionization is avoided whereas the high degree of geometrical alignment is maintained. MRMI, i.e., simultaneous mapping of angular and velocity distributions for fragment ions [26–28], is demonstrated to be a powerful tool for identification of the three isomers of DCE.

2. Experiment and Analysis

2.1. Measurement of Time-of-Flight (TOF) Spectra

Figure 1 shows a schematic diagram of the experimental setup. Linearly polarized femtosecond laser pulses (pulse width ~60 fs, wavelength ~795 nm, pulse energy ~3 mJ/pulse) from a Ti:sapphire laser system (Thales α10US-A, France) at a repetition rate of 10 Hz were led through the neutral density (ND) filter to adjust the pulse energy, and focused in a vacuum chamber by using a plano-convex lens (f = 254 mm at 785 nm). The laser intensity at the focus was estimated on the basis of drift momentum of D_2^+ produced by ionization of gaseous D_2 molecules in a circularly polarized laser field [29,30].

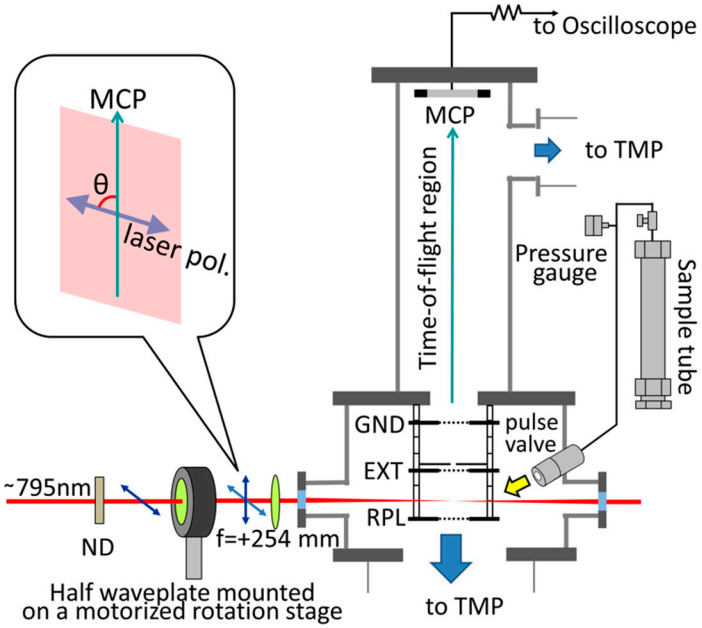


Figure 1. Schematic diagram of the experimental setup; MCP, micro-channel plate; GND, ground electrode; EXT, extracting electrode with a slit; RPL, repelling electrode; ND, neutral density filter; TMP, turbo molecular pump.

Commercially available reagents, 1,1-DCE (Aldrich, 99%, Tokyo, Japan), *cis*-1,2-DCE (Wako Chemicals, 99.0%, Tokyo, Japan), and *trans*-1,2-DCE (Aldrich, 98%, Tokyo, Japan), were degassed by repeated freeze–thaw cycles. The vapor molecules were introduced into the vacuum chamber through a pulsed valve (Parker Hight-Speed Pulse Valve, Series 9, USA). To avoid negative effects on the momentum images due to clustering and space charge effects, the backing pressure of the pulsed valve was kept below 1.3×10^3 Pa. The pressure in the vacuum chamber was below 8×10^{-5} Pa throughout the experiments. The present condition has no relevance to filamentation or plasma-induced terahertz radiation at relatively high pressure [31].

Photoinduced ions at the laser focus were extracted in an electric field of 0.2 kV/cm, then accelerated in the second electric field of 1.9 kV/cm with a standard Wiley–McLaren-type mass spectrometer [32]. In order to avoid concomitant detection of excess ions produced in front of and behind the laser focus, a slit of 0.5 mm was placed on the extraction electrode (EXT) [24]. The ions passing through the slit were mass-separated during the travel through a field-free region of 1.5 m, and detected by a micro-channel-plate detector (MCP, Jordan C-0701, φ 18 mm). The signal was averaged for 1000 laser shots by using a digitizing oscilloscope (LeCroy WaveRunner 104Xi-A, 1 GHz, USA).

For a limited surface area on the MCP detector, only a part of the ions exploding forward and backward to the detector was counted as signals. Taking the detection geometry into account, the ion intensity was plotted as a function of angle θ between the direction of the laser polarization and the direction of the flight axis toward the MCP detector (see the inset in Figure 1) to obtain the angular distribution of fragment ions.

2.2. Analysis

The polarization angle of the linearly polarized laser field was rotated from $\theta = 0°$ to 90° by an interval of 5° using a zeroth-order half-wave plate mounted on a motorized rotary stage (Thorlabs PRM1/MZ8E, USA). A series of time-of-flight (TOF) spectra were recorded by changing the polarization angle, from which the angular distribution was deduced for two fragment ions of $^{35}Cl^+$ and C^{2+}.

Using the same set of TOF spectra, the momentum image (MRMI) was constructed [26–28]. Equation (1) represents the relation between the displacement of flight times, Δt, from

the central position of a peak in the TOF spectrum ($p_{//} = 0$) for a fragment ion and the momentum due to Coulomb explosion, $p_{//}$, in parallel with the flight axis. Transformation from the TOF spectrum to the momentum distribution was performed by Equation (1):

$$p_{//} = qF\Delta t, \quad (1)$$

where q denotes the charge of the fragment ion and F the strength of the extraction electric field [28]. Momentum distributions thus calculated were plotted as a function of the laser polarization angle to obtain a contour map, representing both the angular distribution and the velocity distribution in a single 2D image. To obtain better statistics, the distributions in the positive and negative momentum ranges are averaged and plotted in the first quadrant in the MRMI map. On the basis of the symmetry with respect to the laser polarization direction, the momentum distributions in the three other quadrants are the same as that in the first quadrant.

3. Results

3.1. TOF Spectra

Figure 2 shows TOF spectra for three isomers of DCE under the low-laser-intensity condition, 1.8×10^{14} W/cm^2. Laser polarization is set perpendicular to the flight axis. Each spectrum is normalized to the peak intensity of the ion signal for $C_2H_2{}^{35}Cl_2{}^+$ (m/z 96). Major peaks commonly observed for the three isomers are $C_2H_2Cl_2{}^+$ (m/z 96, 98, 100), $C_2H_2Cl^+$ (m/z 61, 63), C_2HCl^+ (m/z 60, 62), $C_2H_2Cl_2{}^{2+}$ (m/z 48, 49, 50), and $C_2H_2{}^+$ (m/z 26). Minor but important peaks are noted for atomic ions of Cl^+ (m/z 35, 37), C^+ (m/z 12), C^{2+} (m/z 6), and H^+ (m/z 1).

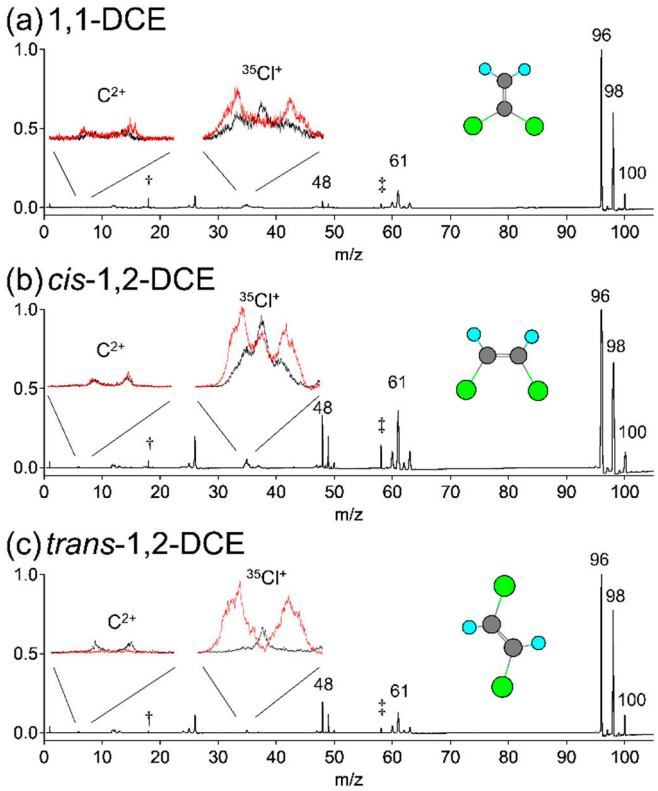


Figure 2. TOF mass spectra of dichloroethylene isomers obtained at the laser intensity of 1.8×10^{14} W/cm^2. Inset spectra show detailed profiles for C^{2+} and $^{35}Cl^+$. Traces in black correspond to laser polarization perpendicular to the flight axis, while traces in red parallel to the flight axis. Peaks with daggers are due to impurities: water (m/z 18) and acetone (m/z 58). Molecular structures are depicted for the three dichloroethylene isomers; Carbon atoms in gray, hydrogen atoms in light blue, and chlorine atoms in green.

Inset spectra in Figure 2 depict split TOF profiles for C^{2+} and $^{35}Cl^{+}$ as a result of Coulomb explosion. In a multiply charged molecular ion, nascent ionic fragments recoil to each other by repulsive forces to leave the center of mass of the molecular framework, acquiring additional velocity components. Deviation, Δt, from the center of symmetry of the TOF peak profile is proportional to the magnitude of parallel momentum, $p_{//}$, forward or backward with respect to the direction toward the MCP detector (See Equation (1) for the relation between the magnitude of momentum and the splitting). Traces in red are the spectra with laser polarization parallel to the flight axis. A split pair of peaks for $^{35}Cl^{+}$ is commonly observed for the three isomers of DCE, as seen in traces in red in Figure 2a–c. Black traces of $^{35}Cl^{+}$, for which laser polarization is perpendicular to the extraction electric field show smaller splitting in Figure 2a,b or no split component in Figure 2c. The smaller the splitting, the slower the velocity acquired from the Coulomb explosion.

For two selected ion signals of $^{35}Cl^{+}$ (m/z 35) and C^{2+} (m/z 6), angular distributions are obtained from a series of the TOF data measured in the present work and compared with those in the preceding work [24]. Concerning the signal at m/z 12 mainly of C^{+}, possibilities of overlapping signals of doubly charged carbon dimer ions of $C_2{}^{2+}$, and triply charged chlorine ions of $^{35}Cl^{3+}$ (m/z 11.7) and $^{37}Cl^{3+}$ (m/z 12.3) cannot be ruled out. Thus, we choose C^{2+} rather than C^{+}.

3.2. Angular Distribution

$^{35}Cl^{+}$: Angular distributions of $^{35}Cl^{+}$ generated upon Coulomb explosion are shown in Figure 3 for three isomers of DCE. At a glance, *trans*-1,2-DCE can be easily identified by its little intensity in the direction of ±90° both under the high- (Figure 3c) and low- (Figure 3f) laser-intensity conditions. In contrast, it seems to be difficult to distinguish 1,1-DCE (Figure 3a,d) from *cis*-1,2-DCE (Figure 3b,e). At this point, the situation has not been very much improved for identification of the isomers. Our new experimental data on $^{35}Cl^{+}$ in Figure 3 merely reproduce the reported angular distributions [24].

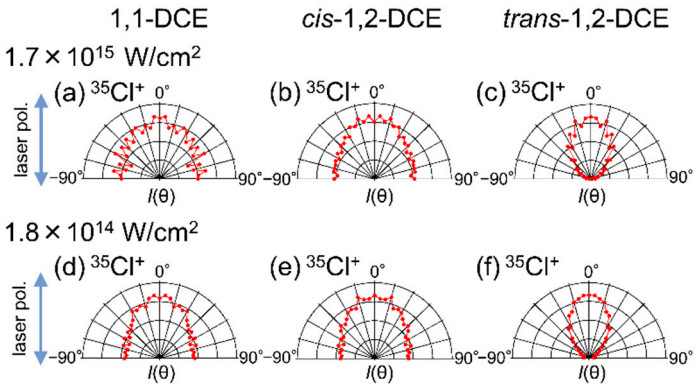


Figure 3. Angular distributions of $^{35}Cl^{+}$ generated from 1,1-DCE (**a**,**d**), *cis*-1,2-DCE (**b**,**e**), and *trans*-1,2-DCE (**c**,**f**). Laser intensities are 1.7 × 10^{15} W/cm^2 for (**a**–**c**) and 1.8 × 10^{14} W/cm^2 for (**d**–**f**). The vertical arrows represent the direction of laser polarization.

In more detail, under the high-laser-intensity condition in Figure 3a–c, 1,1-DCE (Figure 3a) exhibits non-vanishing components in all directions, larger by a factor of ~1.5 in 0° (parallel) than in ±90° (perpendicular). Similar distribution is observed for *cis*-1,2-DCE (3b). A qualitative difference is noted for *trans*-1,2-DCE (Figure 3c), exhibiting an anisotropic distribution with a strong parallel component at 0° and no perpendicular component at ±90°, indicating that the $^{35}Cl^{+}$ ion in *trans*-1,2-DCE is ejected solely along the direction parallel to the laser polarization.

The characteristic feature under the high-laser-intensity condition is found also under the low-laser-intensity condition in Figure 3d–f. Two isomers, 1,1-DCE (Figure 3d) and *cis*-1,2-DCE (Figure 3e), exhibit oval distribution, having a slightly larger component in the parallel direction at 0°. In contrast, *trans*-1,2-DCE (Figure 3f) exhibits again a distinctly

different distribution from the other two isomers. The predominating distribution at 0° with little component at ±90° for $^{35}Cl^+$ (Figure 3f) is similar to that observed under the high-laser-intensity condition (Figure 3c). From the angular distribution of $^{35}Cl^+$, *trans*-1,2-DCE can be identified, but discrimination between 1,1-DCE and *cis*-1,2-DCE remains difficult.

C^{2+}: Under the high-laser-intensity condition at 1.7×10^{15} W/cm^2 in Figure 4, angular distributions of C^{2+} for 1,1-DCE (Figure 4a) and *cis*-1,2-DCE (Figure 4b) resemble each other, i.e., a larger component in 0° (parallel), whereas isotropic distribution is noted for *trans*-1,2-DCE (Figure 4c). According to the preceding work, *trans*-1,2-DCE releases more C^{2+} ions into the direction perpendicular to the laser polarization under the moderate laser intensity at 1.3×10^{15} W/cm^2, whereas an isotropic distribution is seen under the extremely high laser intensity at 2.2×10^{15} W/cm^2 [24]. The present experimental condition, 1.7×10^{15} W/cm^2, falls in-between the two conditions in the literature [24], and our result is close to the latter extremity, as shown in Figure 3c.

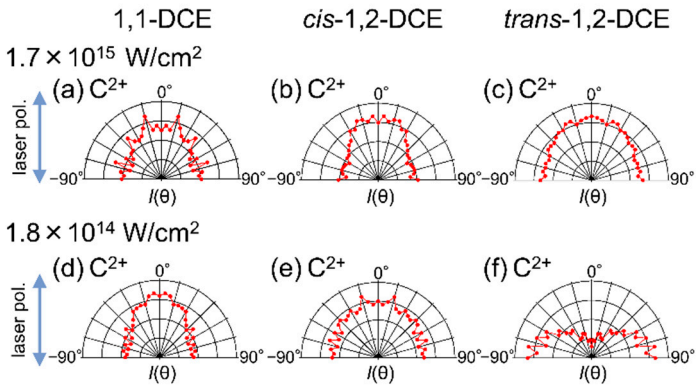


Figure 4. Angular distributions of C^{2+} generated from 1,1-DCE (**a**,**d**), *cis*-1,2-DCE (**b**,**e**), and *trans*-1,2-DCE (**c**,**f**). Laser intensities are 1.7×10^{15} W/cm^2 for (**a**–**c**) and 1.8×10^{14} W/cm^2 for (**d**–**f**). The vertical arrows represent the direction of laser polarization.

It is noted that the angular distribution of C^{2+} for *trans*-1,2-DCE changes dramatically by lowering the laser intensity to 1.8×10^{14} W/cm^2. In Figure 4f, C^{2+} ions are emitted mostly in the direction perpendicular to the laser polarization at the angle of ±90° and little emission is seen in the parallel direction at 0°. Even under the condition at the low laser intensity, a difference is not noticeable in Figure 4d,e. Thus, discrimination of the isomers between 1,1-DCE and *cis*-1,2-DCE is impossible from the angular distribution of the C^{2+} fragment ion.

3.3. Momentum Image

$^{35}Cl^+$: Using the series of the TOF data used for Figures 3 and 4, MRMI analysis is performed for $^{35}Cl^+$ and C^{2+}. Since the TOF signals of $^{35}Cl^+$ and C^{2+} are well-separated from those of the other ionic species, clean momentum images are obtained. Momentum images of $^{35}Cl^+$ are presented in Figure 5. In addition to the angular distribution of momentum, the magnitude of momentum for the leaving ion is represented by distance from the origin, i.e., faster at the outer rim and slower around the center. The contour plot stands for the population of ions having a specific direction and a specific velocity. Independently on the laser intensity, two components are discernible in the momentum images for 1,1-DCE (Figure 5a,d) and *cis*-1,2-DCE (Figure 5b,e), i.e., one for the fast ions traveling forward or backward along the laser polarization, which appear as a split pair of spots at the upper and lower parts of the image, and the other for the slow ions spreading around the center of the image. Therefore, the momentum image of $^{35}Cl^+$ is not sufficient to distinguish 1,1-DCE and *cis*-1,2-DCE. In the momentum images for *trans*-1,2-DCE (Figure 5c,f), only the component of fast ions is discernible along the parallel laser polarization without any slow component.

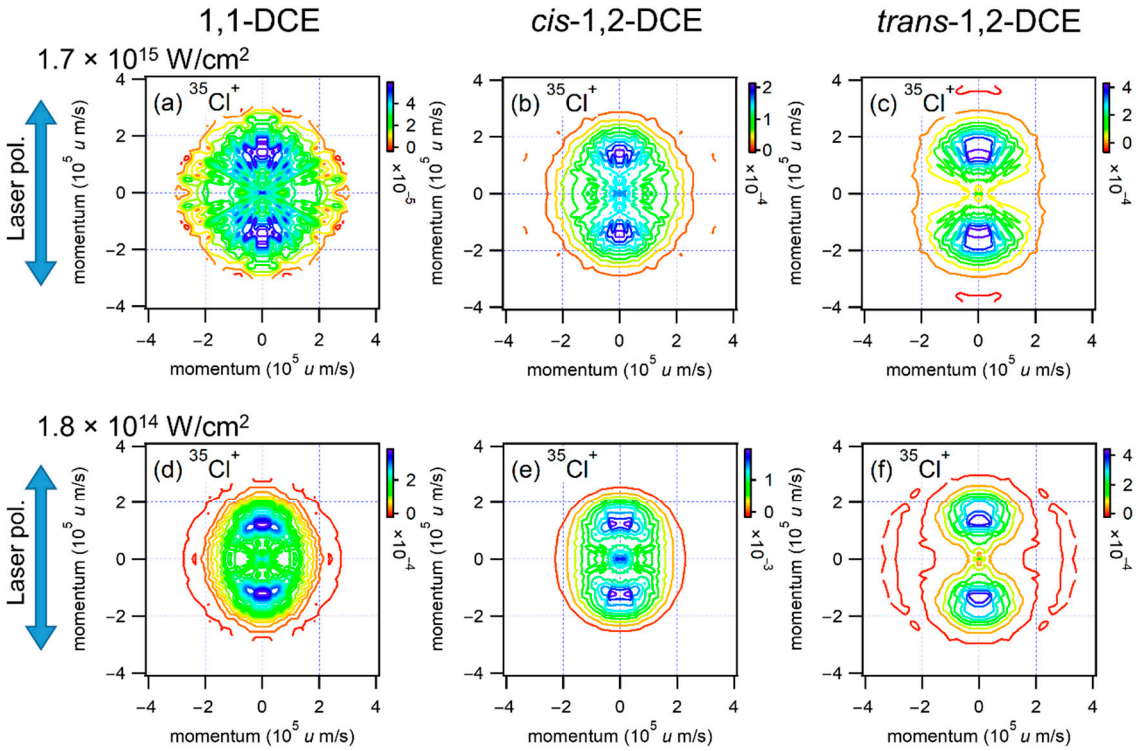


Figure 5. Momentum images of $^{35}Cl^+$ generated from 1,1-DCE (**a**,**d**), *cis*-1,2-DCE (**b**,**e**), and *trans*-1,2-DCE (**c**,**f**). Laser intensities are 1.7 × 10^{15} W/cm^2 for (**a**–**c**) and 1.8 × 10^{14} W/cm^2 for (**d**–**f**). The vertical arrows represent the direction of laser polarization.

C^{2+}: Using momentum images of C^{2+} in Figure 6, appreciable difference between two isomers of 1,1-DCE and *cis*-1,2-DCE is noticed. The image of C^{2+} for 1,1-DCE (Figure 6a) under the high-laser-intensity condition at 1.7 × 10^{15} W/cm^2 contains at least two groups of ions, i.e., a group of fast ions slightly polarized in parallel with laser polarization and a group of slow ions locating near the center of the image, as is seen more clearly under the low laser intensity condition in Figure 6d. On the other hand, for *cis*-1,2-DCE (Figure 6b) and *trans*-1,2-DCE (Figure 6c), a single component of rather isotropic angular distribution is conspicuous, demonstrating a visible difference between 1,1-DCE (Figure 6a) and the *cis* (Figure 6b) and *trans* (Figure 6c) isomers of 1,2-DCE.

At the appropriately low laser intensity, namely, 1.8 × 10^{14} W/cm^2, momentum images for the three isomers in DCE clearly show different patterns as shown in Figure 6d–f. First, the image of C^{2+} for 1,1-DCE (Figure 6d) shows again the groups of fast and slow ions. Second, the image for *cis*-1,2-DCE (Figure 6e) shows a single velocity component of fast ions whose angular distribution is almost isotropic and slightly polarized in the direction along the laser polarization. Finally, a drastic change is noted in the image of C^{2+} for *trans*-1,2-DCE (Figure 6f). The single velocity component of fast ions in Figure 6f directs perpendicularly to the laser polarization, exhibiting a sharp contrast to the observation of the isotropic distribution in the high laser-intensity counterpart in Figure 6c.

The magnitude of the momentum, 2.0 × 10^5 *u* m/s, for *trans*-1,2-DCE at the pair of spots with maximum population in Figure 6f, is appreciably smaller than that in Figure 6c, 2.7 × 10^5 *u* m/s. This implies that the total charge number of the cation is smaller and/or that enhanced ionization at a deformed molecular structure [33,34] takes place predominantly at the low-laser-intensity condition.

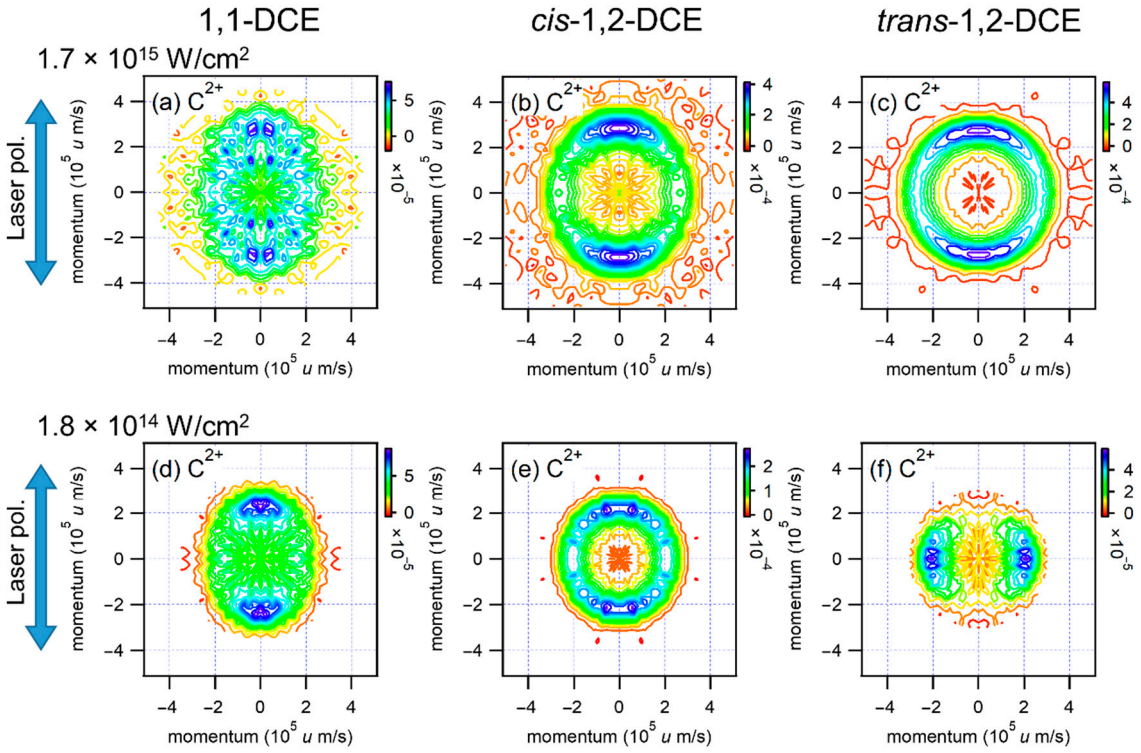


Figure 6. Momentum images of C^{2+} generated from 1,1-DCE (**a**,**d**), *cis*-1,2-DCE (**b**,**e**), and *trans*-1,2-DCE (**c**,**f**). Laser intensities are 1.7×10^{15} W/cm^2 for (**a**–**c**) and 1.8×10^{14} W/cm^2 for (**d**–**f**). The vertical arrows represent the direction of laser polarization.

Using the momentum image of the C^{2+}, it is possible to discern the structural isomer of 1,1-DCE from the *cis* and *trans* isomers of 1,2-DCE, even under the relatively high-laser-intensity condition. Furthermore, by lowering the laser intensity, in addition to the 1,1-DCE isomer, the pair of *cis* and *trans* isomers of 1,2-DCE can be distinguished by differently polarized emission of C^{2+}, i.e., isotropic but slightly polarized in parallel with the laser polarization for *cis*-1,2-DCE and perpendicularly polarized emission of C^{2+} from *trans*-1,2-DCE, as evidenced by the series of momentum images in Figure 6d–f. Under the laser intensity at 1.8×10^{14} W/cm^2, it is demonstrated that all the three isomers in DCE can be identified by the momentum images of the C^{2+} fragment ion.

4. Discussion

The laser polarization can select molecules at specific orientation upon ionization with a short laser pulse, whereby only a fraction of molecules is preferentially ionized into multiply charged ions for Coulomb explosion. In this case, the angular distribution of fragment ions reflects intrinsic anisotropy of the parent molecule. This selection of molecular *geometrical alignment*, or the idea of a preferential *ionization axis*, was proposed for DCE isomers [24,35,36]. Geometrical alignment is determined by orientation-dependent probability of ionization, which primarily depends on the shape of the outer edge of a molecular orbital with respect to the laser polarization [37,38]. However, in the case of multiple ionization, it is difficult to identify which orbitals are contributing. Furthermore, when the chemical bond can be elongated to possibly twice the bond length for the equilibrium geometry in the neutral ground state within the exposure time of an intense laser pulse, probability of multiple ionization is significantly enhanced at an alignment angle in which the chemical bond is parallel to the laser electric field [39]. In addition, dynamical alignment by the interaction between the induced dipole moment and the laser electric field influences significantly the angular distribution of the recoiled fragment ions [40–43].

Here, we discuss the momentum distribution of fragment ions of DCE isomers on the basis of the specific molecular orientation upon ionization. We simply assume that

the molecules whose most polarizable axis is oriented along the laser polarization are preferentially ionized into multiply charged ions. Anisotropic nature of polarizability of a molecule is represented by a tensor property. The six components of the polarizability tensor, α, are diagonalized to three orthogonal components along the principal axes of the ellipsoid. For a molecule of DCE isomers, two of them along the molecular plane, α_{xx} and α_{yy}, have characteristic values of 42–82 in the unit of cubic Bohr radius, a_0^3, whereas the other component perpendicular to the molecular plane, α_{zz}, is smaller than the two, having a value of ~33.7 commonly for the three DCE isomers [44]. In this work, the principal axis of the largest polarizability among the three components is defined as the *most polarizable axis* of the target molecule, which is indicated by the solid red arrow in each of Figure 7a–c.

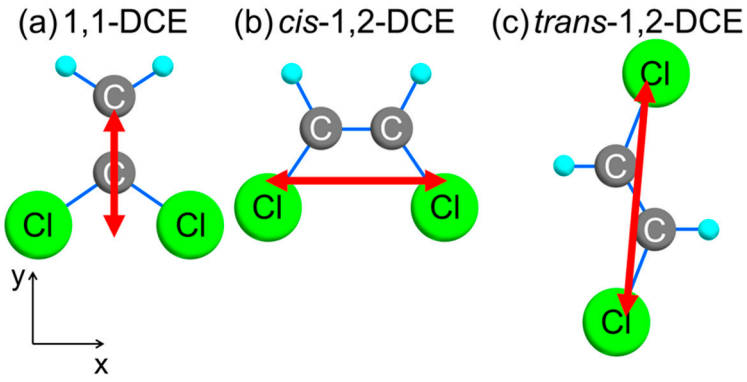


Figure 7. The largest component of polarizability along the principal axis (red arrow) evaluated for (**a**) 1,1-DCE, (**b**) *cis*-1,2-DCE, and (**c**) *trans*-1,2-DCE isomers by density functional theory calculations [44].

4.1. Momentum Distribution of $^{35}Cl^+$

Having the momentum parallel to the laser polarization, the fast component of the fragment ion, Cl^+, commonly observed for the three isomers of DCE, is released upon ionization of the molecule aligned along the relevant C–Cl bond. Since the leaving Cl^+ ion is located at an edge of the molecular framework, the nascent molecular ion of minimum charges for Coulomb explosion is Cl^+-$(C_2H_2Cl)^+$. The slow component of the fragment ion, Cl^+, observed for 1,1-DCE in Figure 5a,d and for *cis*-1,2-DCE in Figure 5b,e is possibly a superposition of Cl^+ signals from singly charged molecular ions, Cl^+-C_2H_2Cl. The parallel release of the fast Cl^+ ions to the laser polarization might have relevance to the most polarizable axis for *cis*-1,2-DCE in Figure 7b and for *trans*-1,2-DCE in Figure 7c (solid arrows in red). However, the close resemblance of split patterns in Figure 5a–f rather indicates a common mechanism where the molecule aligned with its C–Cl bond axis parallel to the laser axis is preferentially ionized into the least multiply charged repulsive pair of ions, C^+ and Cl^+, for Coulomb explosion. This molecular geometrical alignment along the C–Cl bond is compatible qualitatively with the ionization axis discussed previously [24].

4.2. Momentum Distribution of C^{2+}

For the doubly charged fragment ion, C^{2+}, more than three charges, >+3*e*, are expected for the molecular ion. The momentum images of C^{2+} show appreciable differences between 1,1-DCE (Figure 6a,d) and *cis*-1,2-DCE (Figure 6b,e), which are explainable by the difference in relative positions of carbon atoms in a molecule. In 1,1-DCE, one carbon atom is bonded to two chlorine atoms and the other is located away from the chlorine atoms. The former, locating close to the molecular center of mass, contributes to the isotropic low-velocity (slow) component, and the latter, located at the edge of a molecule, contributes to the anisotropic high-velocity (fast) component. As a result, two types of components emerge in the momentum image in Figure 6a,d. In *cis*-1,2-DCE, each of the two carbon atoms is bonded to one chlorine atom and both are equivalent in a molecule, and thus the majority of C^{2+} fragment ions from *cis*-1,2-DCE constitute a single-velocity component in Figure 6b,e.

The momentum image of C^{2+} for *trans*-1,2-DCE in Figure 6f at the low-laser-intensity condition shows a pattern extending in the direction perpendicular to the laser polarization. This makes a sharp contrast to those of C^{2+} for the other two isomers in Figure 6d,e, which extend more or less in parallel with the direction of laser polarization. To cause C^{2+} to be Coulomb-exploded, at least one counter cation, namely, a carbon or chlorine ion, is necessary. Regardless of which ion is the counterpart, the repulsive force will point in a direction rather parallel to the laser polarization, considering the stable structure shown in Figure 7c. However, heavy chlorine nuclei locating along the most polarizable axis force the C^{2+} ion to leave more or less perpendicularly to the axis of laser polarization. The Cl nuclei move slower than the C^{2+} ion because the mass of Cl (m = 35 or 37) is roughly three times heavier than that of ^{12}C. Thus, the Cl nuclei stay longer near the molecular center of mass, preventing the C^{2+} from leaving in the direction parallel to the laser polarization. The disturbance by Cl nuclei will cause the trajectory of C^{2+} to be bent, resulting in deviation from the expected momentum distribution on the basis of the initial geometrical structure. The structural deformation also causes deviated momentum distribution [33,34]. Nevertheless, the initial acceleration determines overall properties of the Coulomb explosion event.

4.3. Molecular Structure Assay

The momentum image of $^{35}Cl^{+}$ fragment ions obtained in the present work represents molecular geometrical alignment along the C–Cl bond of the molecule. Moreover, the momentum image of C^{2+} reflects the relative position of multiply charged fragment ions in a highly charged molecule. A key feature to be noted is to conduct experiments under the condition at the lowest possible laser intensity, as long as sufficient signal counts of fragment ions formed by Coulomb explosion are detectable, where the number of ionization channels is reduced and the intrinsic anisotropy is maximized in MRMI. Ultra-short laser pulses, <10 fs, would be advantageous to surmise a molecular structure from MRMI by avoiding extensive deformation [3–6,33,34], enhanced ionization [39], and dynamical alignment [40–43] of molecules prior to Coulomb explosion. A combination of MRMI with laser-induced alignment might be helpful for applying this method for other molecules and/or to determine molecular structure more precisely, as shown previously [22,23]. Although one should relent on locating the position of hydrogen atoms in a molecule because of their migration being inevitably large [45–47], it will not be a serious problem as it can be reasonably guessed from the position of heavier atoms.

5. Conclusions

According to the different momentum distributions of $^{35}Cl^{+}$, *trans*-1,2-DCE was easily discriminated from the other two. Moreover, the momentum image of C^{2+} enabled us to identify all the three isomers by intensifying the difference in anisotropic distributions between the pair of structural isomers, *cis*-1,2-DCE and 1,1-DCE. Mass-resolved momentum imaging, MRMI, was demonstrated to reflect the difference in the location of constituent atoms in a molecule. This, in turn, implies a potential application of MRMI to acquiring information that enables one to reconstruct the relative position of constituent atoms in a molecule, namely, the molecular structure. The analysis of MRMI can be exploited to guess unknown structures of molecular species as long as their chemical compositions are known.

Author Contributions: Conceptualization, R.I. and T.W.; investigation, Y.W., H.A. and T.K.; data curation, Y.W.; visualization, Y.W.; writing—original draft preparation, Y.W. and T.W.; writing—review and editing, H.A. and R.I.; funding acquisition, R.I. and T.W. All authors have read and agreed to the published version of the manuscript.

Funding: This study is partly supported by JSPS KAKENHI (Grant No. JP26288013) and MEXT—Supported Program for the Strategic Research Foundation at Private Universities.

Institutional Review Board Statement: Not applicable.

Informed Consent Statement: Not applicable.

Data Availability Statement: The data presented in this study are available upon request from the corresponding author.

Acknowledgments: The authors are grateful to Y. Hagihara for support in data analysis. The authors thank M. Nishikino and N. Hasegawa for the support in laser operation. Y.W. acknowledges Grant-in-Aid for JSPS Research Fellow (Grant No. JP24-10606).

Conflicts of Interest: The authors declare no conflict of interest.

References

1. Vager, Z.; Naaman, R.; Kanter, E.P. Coulomb explosion imaging of small molecules. *Science* **1989**, *244*, 426–431. [CrossRef]
2. Herwig, P.; Zawatzky, K.; Grieser, M.; Heber, O.; Jordon-Thaden, B.; Krantz, C.; Novotný, O.; Repnow, R.; Schurig, V.; Schwalm, D.; et al. Imaging the absolute configuration of a chiral epoxide in the gas phase. *Science* **2013**, *342*, 1084–1086. [CrossRef] [PubMed]
3. Sanderson, J.H.; El-Zein, A.; Bryan, W.A.; Newell, W.R.; Langley, A.J.; Taday, P.E. Geometry modifications and alignment of H_2O in an intense femtosecond laser pulse. *Phys. Rev. A* **1999**, *59*, R2567–R2570. [CrossRef]
4. Légaré, F.; Lee, K.F.; Litvinyuk, I.V.; Dooley, P.W.; Wesolowski, S.S.; Bunker, P.R.; Dombi, P.; Krausz, F.; Badrauk, A.D.; Villeneuve, D.M.; et al. Laser Coulomb explosion imaging of small molecules. *Phys. Rev. A* **2005**, *71*, 013415. [CrossRef]
5. Hasegawa, H.; Hishikawa, A.; Yamanouchi, K. Coincidence imaging of Coulomb explosion of CS_2 in intense laser fields. *Chem. Phys. Lett.* **2001**, *349*, 57–63. [CrossRef]
6. Gagnon, J.; Lee, K.F.; Rayner, D.M.; Corkum, P.B.; Bhardwaj, V.R. Coincidence imaging of polyatomic molecules via laser-induced Coulomb explosion. *J. Phys. B At. Mol. Opt. Phys.* **2008**, *41*, 215104. [CrossRef]
7. Wu, J.; Kunitski, M.; Schmidt, L.P.H.; Jahnke, T.; Dörner, R. Structures of N_2Ar, O_2Ar, and O_2Xe dimers studied by Coulomb explosion imaging. *J. Chem. Phys.* **2012**, *137*, 104308. [CrossRef]
8. Slater, C.S.; Blake, S.; Brouard, M.; Lauer, A.; Vallance, C.; John, J.J.; Turchetta, R.; Nomerotski, A.; Christensen, L.; Nielsen, J.H.; et al. Covariance imaging experiments using a pixel-imaging mass-spectrometry camera. *Phys. Rev. A* **2014**, *89*, 11401. [CrossRef]
9. Tanaka, H.; Nakashima, N.; Yatsuhashi, T. Anisotropic Coulomb explosion of CO ligands in group 6 metal hexacarbonyls: $Cr(CO)_6$, $Mo(CO)_6$, $W(CO)_6$. *J. Phys. Chem. A* **2016**, *120*, 6917–6928. [CrossRef]
10. Mathur, D. Structure and dynamics of molecules in high charge states. *Phys. Rep.* **2004**, *391*, 1–118. [CrossRef]
11. Castleman, A.W.; Bowen, K.H. Clusters: Structures, energies, and dynamics of intermediate states of matter. *J. Phys. Chem.* **1996**, *100*, 12911–12944.
12. Wakabayashi, T.; Ong, A.-L.; Strelnikov, D.; Krätschmer, W. Flashing carbon on cold surfaces. *J. Phys. Chem. B* **2004**, *108*, 3686–3690. [CrossRef]
13. Wada, Y.; Wakabayashi, T.; Kato, T. Photoinduced reaction of hydrogen-end-capped polyynes with iodine molecules. *J. Phys. Chem. B* **2011**, *115*, 8439–8445. [CrossRef] [PubMed]
14. Wada, Y.; Morisawa, Y.; Wakabayashi, T. Spectroscopic characterization of a series of polyyne-iodine molecular complexes of $H(C{\equiv}C)_nH(I_6)$ n=5-9. *Chem. Phys. Lett.* **2012**, *541*, 54–59. [CrossRef]
15. Wada, Y.; Koma, K.; Ohnishi, Y.; Sasaki, Y.; Wakabayashi, T. Photoinduced reaction of methylpolyynes $H(C{\equiv}C)_nCH_3$ (n=5-7) and $H(C{\equiv}C)_nH$ with I_2 molecules. *Eur. J. Phys. D* **2012**, *66*, 322. [CrossRef]
16. Mitsubayashi, N.; Yatsuhashi, T.; Tanaka, H.; Furukawa, S.; Kozai, M.; Okada, K.; Nakashima, N. Anisotropic Coulomb explosion of acetylene and diacetylene derivatives. *Int. J. Mass Spetrom.* **2016**, *403*, 43–52. [CrossRef]
17. Pitzer, M.; Kunitski, M.; Johnson, A.S.; Jahnke, T.; Sann, H.; Sturm, F.; Schmidt, L.P.H.; Schmidt-Böcking, H.; Dörner, R.; Stohner, J.; et al. Direct determination of absolute molecular stereochemistry in gas phase Coulomb explosion imaging. *Science* **2013**, *341*, 1096–1100. [CrossRef]
18. Pitzer, M.; Kastirke, G.; Burzynski, P.; Weller, M.; Metz, D.; Neff, J.; Waitz, M.; Trinter, F.; Schmidt, L.P.H.; Williams, J.B.; et al. Stereochemical configuration and selective excitation of the chiral molecule halothane. *J. Phys. B At. Mol. Opt. Phys.* **2016**, *49*, 234001. [CrossRef]
19. Pitzer, M.; Kastirke, G.; Kunitski, M.; Jahnke, T.; Bauer, T.; Goihl, C.; Trinter, F.; Schober, C.; Henrichs, K.; Becht, J.; et al. Absolute configuration from different multifragmentation pathways in light-induced Coulomb explosion imaging. *ChemPhysChem* **2016**, *17*, 2465–2472. [CrossRef]
20. Kitamura, T.; Nishide, T.; Shiromaru, H.; Achiba, Y.; Kobayashi, N. Direct observation of "dynamic" chirality by Coulomb explosion imaging. *J. Chem. Phys.* **2001**, *115*, 5–6. [CrossRef]
21. Ablikim, U.; Bomme, C.; Savelyev, E.; Xiong, H.; Kushawaha, R.; Boll, R.; Amini, K.; Osipov, T.; Kilcoyne, D.; Rudenko, A.; et al. Isomer-dependent fragmentation dynamics of inner-shell photoionized difluoroiodobenzene. *Phys. Chem. Chem. Phys.* **2017**, *19*, 13419–13431. [CrossRef] [PubMed]
22. Christensen, L.; Nielsen, J.H.; Slater, C.S.; Lauer, A.; Brouard, M.; Stapelfeldt, H. Using laser-induced Coulomb explosion of aligned chiral molecules to determine their absolute configuration. *Phys. Rev. A* **2015**, *92*, 033411. [CrossRef]

23. Burt, M.; Amini, K.; Lee, J.W.L.; Christiansen, L.; Johansen, R.R.; Kobayashi, Y.; Pickering, J.D.; Vallance, C.; Brouard, M.; Stapelfeldt, H. Communication: Gas-phase structural isomer identification by Coulomb explosion of aligned molecules. *J. Chem. Phys.* **2018**, *148*, 091102. [CrossRef]
24. Yatsuhashi, T.; Nakashima, N.; Azuma, J. Coulomb explosion of dichroloethylene geometric isomers at 1 PW cm^{-2}. *J. Phys. Chem. A* **2013**, *117*, 1393–1399. [CrossRef]
25. Ablikim, U.; Bomme, C.; Xiong, H.; Savelyev, E.; Obaid, R.; Kaderiya, B.; Augustin, S.; Schnorr, K.; Dumitriu, I.; Osipov, T.; et al. Identification of absolute geometries of cis and trans molecular isomers by Coulomb explosion imaging. *Sci. Rep.* **2016**, *6*, 38202. [CrossRef]
26. Hishikawa, A.; Iwamae, A.; Hoshina, K.; Kono, M.; Yamanouchi, K. Mass-resolved two-dimensional momentum imaging of the Coulomb explosion of N_2 and SO_2 in an intense laser field. *Chem. Phys. Lett.* **1998**, *282*, 283–291. [CrossRef]
27. Hishikawa, A.; Iwamae, A.; Hoshina, K.; Kono, M.; Yamanouchi, K. Coulomb explosion dynamics of N_2 in intense laser field by mass-resolved momentum imaging. *Chem. Phys.* **1998**, *231*, 315–329. [CrossRef]
28. Iwamae, A.; Hishikawa, A.; Yamanouchi, K. Extraction of molecular dynamics in intense laser fields from mass-resolved momentum imaging maps: Application to Coulomb explosion of NO. *J. Phys. B At. Mol. Opt. Phys.* **2000**, *33*, 223–240. [CrossRef]
29. Litvinyuk, I.V.; Lee, K.F.; Dooley, P.W.; Rayner, D.M.; Villeneuve, D.M.; Corkum, P.B. Alignment-dependent strong field ionization of molecules. *Phys. Rev. Lett.* **2003**, *90*, 233003. [CrossRef]
30. Alnaser, A.S.; Tong, X.M.; Osipov, T.; Voss, S.; Maharjan, C.M.; Shan, B.; Chang, Z.; Cocke, C.L. Laser-peak-intensity calibration using recoil-ion momentum imaging. *Phys. Rev. A* **2004**, *70*, 023413. [CrossRef]
31. Jahangri, F.; Hashida, M.; Tokita, S.; Nagashima, T.; Hangyo, M.; Sakabe, S. Enhancing the energy of terahertz radiation from plasma-produced by intense femtosecond laser pulses. *Appl. Phys. Lett.* **2013**, *102*, 191106. [CrossRef]
32. Wiley, W.C.; McLaren, I.H. Time-of-flight mass spectrometer with improved resolution. *Rev. Sci. Instrum.* **1955**, *26*, 1150. [CrossRef]
33. Hishikawa, A.; Iwamae, A.; Yamanouchi, K. Ultrafast deformation of the geometrical structure of CO_2 induced in intense laser fields. *Phys. Rev. Lett.* **1999**, *83*, 1127–1130. [CrossRef]
34. Hishikawa, A.; Iwamae, A.; Yamanouchi, K. Ultrafast structural deformation of NO_2 in intense laser fields studied by mass-resolved momentum imaging. *J. Chem. Phys.* **1999**, *111*, 8871–8878. [CrossRef]
35. Wong, M.C.H.; Brichta, J.-P.; Spanner, M.; Patchkovskii, S.; Bhardwaj, V.R. High-harmonic spectroscopy of molecular isomers. *Phys. Rev. A* **2011**, *84*, 051403, Erratum in *Phys. Rev. A* **2012**, *85*, 049901. [CrossRef]
36. Le, A.-T.; Lucchese, R.R.; Lin, C.D. High-order harmonic generation from molecular isomers with midinfrared intense laser pulses. *Phys. Rev. A* **2013**, *88*, 021402. [CrossRef]
37. Tong, X.M.; Zhao, Z.X.; Lin, C.D. Theory of molecular tunneling ionization. *Phys. Rev. A* **2002**, *66*, 033402. [CrossRef]
38. Alnaser, A.S.; Voss, S.; Tong, X.M.; Maharjan, C.M.; Ranitovic, P.; Ulrich, B.; Osipov, T.; Shan, B.; Chang, Z.; Cocke, C.L. Effect of molecular structure on ion disintegration patterns in ionization of O_2 and N_2 by short laser pulses. *Phys. Rev. Lett.* **2004**, *93*, 113003. [CrossRef]
39. Posthumus, J.H.; Giles, A.J.; Thompson, M.R.; Codling, K. Field-ionization, Coulomb explosion of diatomic molecules in intense laser fields. *J. Phys. B* **1996**, *29*, 5811–5829. [CrossRef]
40. Rosca-Pruna, F.; Vrakking, M.J.J. Experimental observation of revival structures in picosecond laser-induced alignment of I_2. *Phys. Rev. Lett.* **2001**, *87*, 153902. [CrossRef]
41. Stapelfeldt, H.; Seideman, T. Colloquium: Aligning molecules with strong laser pulses. *Rev. Mod. Phys.* **2003**, *75*, 543–557. [CrossRef]
42. Tong, X.M.; Zhao, Z.X.; Alnaser, A.S.; Voss, S.; Cocke, C.L.; Lin, C.D. Post ionization alignment of the fragmentation of molecules in an ultrashort intense laser field. *J. Phys. B* **2005**, *38*, 333–341. [CrossRef]
43. Koch, C.P.; Lemeshko, M.; Sugny, D. Quantum control of molecular rotation. *Rev. Mod. Phys.* **2019**, *91*, 035005. [CrossRef]
44. Frisch, M.J.; Trucks, G.W.; Schlegel, H.B.; Scuseria, G.E.; Robb, M.A.; Cheeseman, J.R.; Scalmani, G.; Barone, V.; Petersson, G.A.; Nakatsuji, H.; et al. *B3LYP/6-311++G(2d,p) Optimized Molecular Geometries and Polarizability Tensors for DCE Isomers, Gaussian 16*; Revision A.03; Gaussian, Inc.: Wallingford, CT, USA, 2016.
45. Hishikawa, A.; Matsuda, A.; Fushitani, M.; Takahashi, E. Visualizing recurrently migrating hydrogen in acetylene dication by intense ultrashort laser pulses. *Phys. Rev. Lett.* **2007**, *99*, 258302. [CrossRef]
46. Itakura, R.; Liu, P.; Furukawa, Y.; Okino, T.; Yamanouchi, K.; Nakano, H. Two-body Coulomb explosion and hydrogen migration in methanol induced by intense 7 and 21 fs laser pulses. *J. Chem. Phys.* **2007**, *127*, 104306. [CrossRef] [PubMed]
47. Ibrahim, H.; Wales, B.; Beaulieu, S.; Schmidt, B.E.; Thiré, N.; Fowe, E.P.; Bisson, É.; Hebeisen, C.T.; Wanie, V.; Giguére, M.; et al. Tabletop imaging of structural evolutions in chemical reactions demonstrated for the acetylene cation. *Nat. Commun.* **2014**, *5*, 4422. [CrossRef] [PubMed]